Intensity-Modulated Strain Sensor Based on Fiber In-Line Mach–Zehnder Interferometer

Jiangtao Zhou, Yiping Wang, *Senior Member, IEEE*, Changrui Liao, Guolu Yin, Xi Xu, Kaiming Yang, Xiaoyong Zhong, Qiao Wang, and Zhengyong Li

***Abstract*— We demonstrated a novel intensity-modulated strain sensor based on a fiber in-line Mach–Zehnder interferometer with a large fringe visibility of up to 17 dB, which was fabricated by splicing a section of thin core fiber between two sections of single mode fibers with one misalignment-spliced joint. Such a strain sensor exhibited an ultrahigh sensitivity of −0.023 dBm/$\mu\varepsilon$ within a measurement range of 500 $\mu\varepsilon$, which is about one order of magnitude higher than that reported in references. Displacement and stress distributions at the misalignment spliced joint were simulated by use of finite element method. In addition, the proposed strain sensor has an advantage of compact size of ∼10 mm.**

***Index Terms*— Elasto-optical effect, intensity-modulation, misalignment splicing, physical deformation, strain sensor, thin core fiber.**

I. Introduction

FIBER in-line Mach–Zehnder interferometer (MZI) sensors are having attracted great research interests and widely used in practical industrial engineering and military fields due to their unique advantages, such as compact size, low cost, high sensitivity, and immunity to electromagnetic interference [1]–[3]. So far, many types of fiber MZI configurations have been demonstrated via singlemode-multimode-singlemode (SMS) fiber structure [4], [5], fiber mode field mismatch fusion [6], [7], waist-deformed fiber taper [8], [9], long period fiber gratings (LPFGs) [10]–[13], in-fiber femtosecond laser micromachining [14], [15], microfiber-based structures [16], [17], and photonic crystal fibers (PCFs) [18], [19]. These configurations show good performance in the applications of sensing temperature, strain, curvature and surrounding refractive index. Unfortunately, wavelength modulation, rather than intensity modulation, were employed in almost of MZI-based sensors [20]–[22], which has to require expensive demodulation devices in practical sensing applications.

In this letter, we demonstrated a novel intensity-modulated strain sensor based on a fiber in-line MZI. This MZI was created by splicing a section of thin core fiber (TCF) between two sections of standard single mode fibers (SMFs) with one misaligned spliced joint. Such a strain sensor exhibited an ultrahigh sensitivity of −0.023 dBm/$\mu\varepsilon$ within a measurement range of 500 $\mu\varepsilon$.

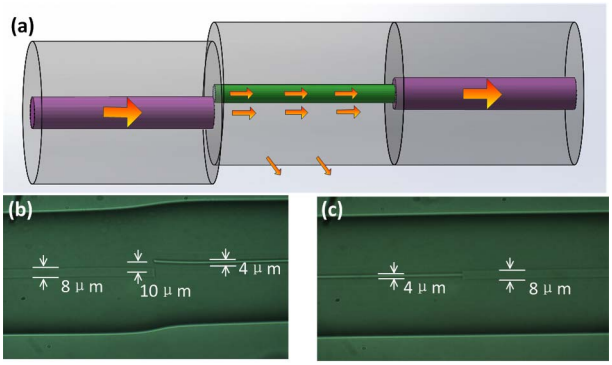

Fig. 1. (a) Fiber in-line MZI structure. Optical microscope images of (b) the lead-in spliced joint with a core offset and (c) the lead-out spliced joint without a core offset.

II. Principle

As shown in Fig. 1(a), a section of TCF is spliced between two sections of SMFs, i.e. so-called the lead-in SMF and the lead-out SMF. A core offset is created at the lead-in spliced joint. Resulting from the core offset, the light propagating from the lead-in SMF is divided into two parts: a fraction of light will propagate into the core of the TCF as a core mode, and majority of light propagate into the cladding of the TCF as a cladding mode. After propagating through the TCF, the two parts of light meet at the lead-out spliced joint and interfere each other in the core of the lead-out SMF [23]–[25], resulting in an interference. The visibility of fringe pattern can be given as [26]:

$$V = 2\alpha \left(\alpha^2 \frac{\gamma}{1-\gamma} + \frac{1-\gamma}{\gamma} \right)^{-1} \quad (1)$$

where γ is the ratio of light emitted into the core of the TCF at the lead-in spliced joint in which light is excited into the

Manuscript received October 22, 2013; revised December 10, 2013; accepted December 16, 2013. Date of publication December 20, 2013; date of current version February 11, 2014. This work was supported in part by the National Science Foundation of China under Grants 11174064, 61308027, and 61377090, in part by the Science and Technology Innovation Commission of Shenzhen under Grants KQCX20120815161444632 and JCYJ20130329140017262, and in part by the Distinguished Professors Funding from Shenzhen University and Guangdong Province Pearl River Scholars. *(Corresponding author: Y. Wang.)*

J. Zhou, Y. Wang, C. Liao, G. Yin, K. Yang, X. Zhong, Q. Wang, and Z. Li are with the Key Laboratory of Optoelectronic Devices and Systems of Ministry of Education and Guangdong Province, Shenzhen University, Shenzhen 518060, China (e-mail: ypwang@szu.edu.cn).

X. Xu is with the College of Civil Engineering, Shenzhen University, Shenzhen 518060, China.

Color versions of one or more of the figures in this letter are available online at http://ieeexplore.ieee.org.

Digital Object Identifier 10.1109/LPT.2013.2295826

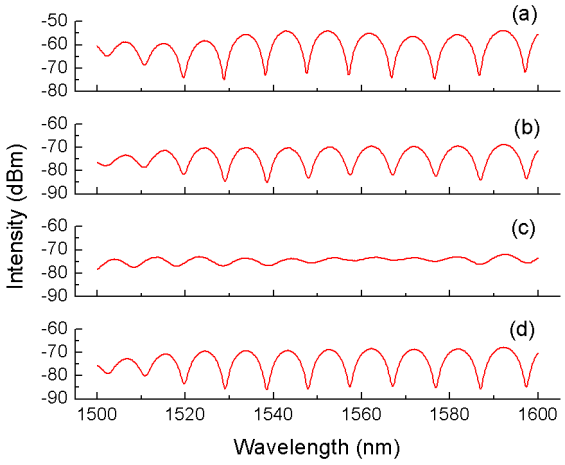

Fig. 2. Interference fringe patterns of the MZI (a) before and (b) after arc discharge was done, (c) after the lead-in spliced joint was removed from the fiber holders in the splicer, and (d) after the MZI was slightly stretched along the fiber axis.

core and cladding modes, and α is the propagation loss of the cladding modes in the TCF and its unit is percentage. It can be easily found from Eq. 1 that the fringe visibility is critically determined by the splitting ratio of γ, which can be carefully adjusted by changing the core offset at the lead-in spliced joint. The strain-induced wavelength shift of fringe dips can be expressed as [7]:

$$\delta\lambda_{dip,\varepsilon} = \frac{2(\Delta n_{eff,\varepsilon} - \delta n_{eff,\varepsilon})(L+\delta L)}{2m+1} - \frac{2\Delta n_{eff,\varepsilon}\cdot L}{2m+1} \approx 2\frac{\Delta n_{eff,\varepsilon}\cdot \delta L - \delta n_{eff,\varepsilon}\cdot L}{2m+1} \quad (2)$$

where L is the length of the TCF, $\Delta n_{eff,\varepsilon}$ is effective refractive index difference between the core mode and the cladding mode at the tensile strain of ε, the $\delta n_{eff,\varepsilon}$ is the strain-induced change of $\Delta n_{eff,\varepsilon}$, the δL is the strain-induced change of the TCF length, and m is the order of the cladding mode.

III. Experiments and Discussion

A. Fabrication of the MZI

First of all, a section of TCF (Nufern UHNA-3) with a length of 8 mm was spliced with the lead-out SMF (Corning SMF-28) without any core offset by a commercial splicer (Fujikura FSM-60s), as illustrated in Fig. 2(c). That is, the lead-out spliced joint was achieved. Secondly, another end of the TCF and the lead-in SMF were fixed by the left and right fiber holders located in the splicer, respectively. Meanwhile, a broadband light source and an optical spectrum analyzer were connected with the lead in/out SMF, respectively, to monitor interference spectrum. Thirdly, the core offset between the lead-in SMF and the TCF was carefully adjusted via the hand mode of the splicer until the best fringe visibility (about 20 dB near the wavelength of 1550 nm) was observed, as shown in Fig. 2(a). Fourthly, arc discharge was done. Consequently, the lead-in spliced joint with a core offset of about 10 μm was created, as illustrated in Fig. 1(b), where the core of

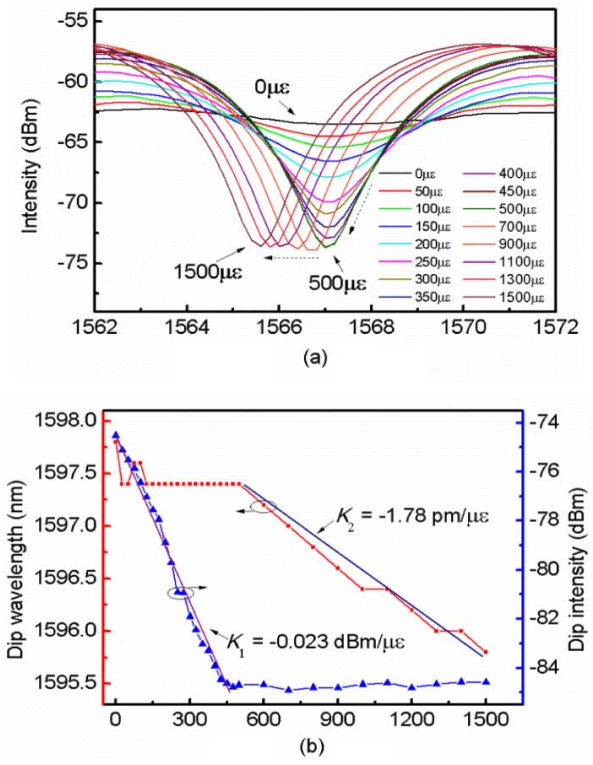

Fig. 3. (a) Interference fringes of the MZI with different tensile strains. (b) Dip wavelength and dip intensity versus tensile strain.

TCF was curved upward slightly, resulting from the splice-induced overlap between the ends of the lead-in SMF and the TCF.

Fig. 2(b) illustrates a fringe pattern observed after arc discharge was done, where the fringe visibility is about 17dB near the wavelength of 1550 nm. As soon as the lead-in spliced joint was removed from the fiber holders in the splicer, poor fringe visibility was observed, as shown in Fig. 2(c), due to the release of the fiber-holder-induced tensile stress in the lead-in spliced joint and the change of the splitting ratio, γ. Furthermore, it is interesting to note that good fringe visibility reappeared, as shown in Fig. 2(d), as soon as the MZI was slightly stretched along the fiber axis. Detailed reason of this unique phenomenon will be discussed in next paragraphs. Therefore, such an M-Z interferometer could be developed a promising strain sensor, as described below.

B. Response to Strain

To investigate the response of the MZI structure to tensile strain, the lead-in SMF of the structure was fixed, and the lead-out SMF was attached to a translation stage with a resolution of 10 μm. Then the MZI was stretched along the fiber axis with a step of 10 μm (namely a strain of 50.0 $\mu\varepsilon$) by means of moving the translation stage to induce a tensile strain of up to 1500 $\mu\varepsilon$, where the length of the stretched fibers, including the lead-in and lead-out SMFs and the TCF, was 200 mm. Typical interference fringe patterns of the MZI with different tensile strains are illustrated in Fig. 3(a), where the tensile strain increases from 0 to 500 $\mu\varepsilon$ with a step of 50 $\mu\varepsilon$ and from 500 to 1500 $\mu\varepsilon$ with a step of 200 $\mu\varepsilon$.

As shown in Fig. 3(a), the fringe visibility was enhanced with an increased tensile strain from 0 to 500 $\mu\varepsilon$, but the center wavelength of interference fringe hardly changed. In contrast, while the tensile strain was increased beyond 500 $\mu\varepsilon$, the fringe visibility hardly changed but the interference fringe exhibited a blue shift.

As shown in Fig. 3(b), the minimum intensity of interference fringe, i.e. dip intensity, linearly decreased with an ultrahigh sensitivity of $K_1 = -0.023$ dBm/$\mu\varepsilon$ while the applied tensile strain was increased from 0 to 500 $\mu\varepsilon$, but the change of the center wavelength of interference fringe, i.e. dip wavelength, was negligible. To the best of our knowledge, this sensitivity is about one order of magnitude higher than that reported in references [27], [28], in which a highly birefringent photonic crystal fiber loop mirror was employed to achieve a strain sensor with a sensitivity of -0.0032 dB/$\mu\varepsilon$. While the tensile strain was increased beyond 500 $\mu\varepsilon$, the dip wavelength shifted toward a shorter wavelength with a sensitivity of $K_2 = 1.78$ pm/$\mu\varepsilon$. Providing an optical power meter with a resolution of 0.01 dB is employed to measure the output power of our MZI-based strain sensor, a high strain resolution of 0.43 $\mu\varepsilon$ could be achieved during strain measurement, which is about one order higher than that (i.e. 3.1 $\mu\varepsilon$) of the strain sensor reported in reference [27]. The above strain experiment of the MZI sample were done five times, and good repeatability was achieved owe to simple and compact MZI structure, strong strength of the lead-in spliced joint, and power stability of the broadband light source employed.

C. Simulated Analysis

As shown in Fig. 4, we simulated stress and displacement distributions at the lead-in spliced joint with a core offset of 10 μm via finite element method. Due to the limit of calculation speed, the simulated misalignment-spliced joint sample has a length of 200 μm. We assume that each end of the misalignment-spliced joint sample are stretched by a displacement of 20 pm. That is, a tensile strain of 200 $\mu\varepsilon$ occurs at the two ends of the spliced joint. The interface between the SMF and the TCF is assumed to be the origin point, as illustrated by white dash line in Fig. 4.

Although uniform stretch force is applied to the two ends of the misalignment-spliced joint to simulate stress and displacement distributions, as shown in Fig. 4(a) and (b), distinct color in each grids indicates that different areas of the joint suffer distinct/asymmetric stress and displacement due to the core offset. In other words, different displacements, namely asymmetric physics deformation, occur near the interface between the SMF and the TCF, as illustrated in Fig. 4(a). And different stress occur in each grids at the spliced joint, as illustrated in Fig. 4(b), which results in a change of refractive index profile at the spliced joint due to elasto-optical effect. Consequently, the change of refractive index profile and asymmetric physics deformation alter the ratio, γ, of light emitted into the core and the cladding of the TCF. As a result, the fringe visibility is effectively modulated, according to Eq. (1). Hence, the dip intensity of interference fringes was linearly decreased

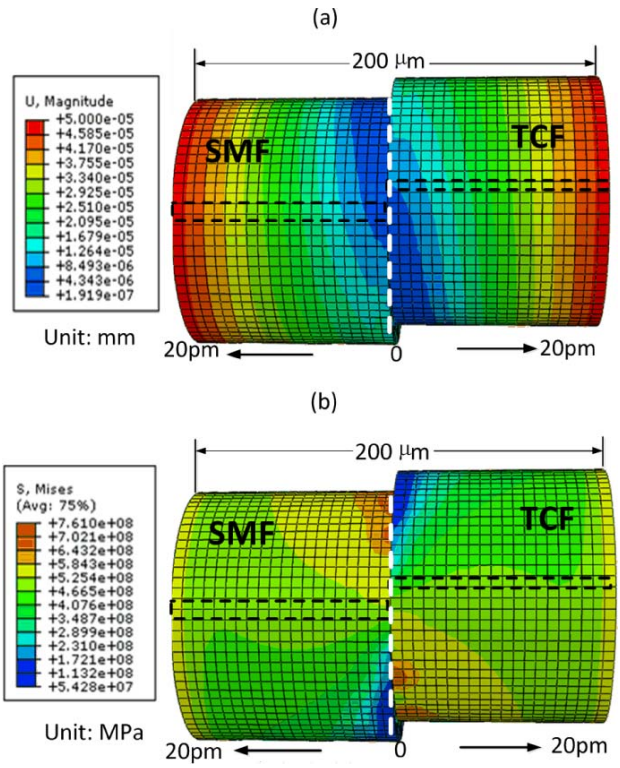

Fig. 4. Simulated (a) displacement and (b) stress distributions at the lead-in spliced joint with a core offset of 10 μm under a tensile strain of 200 $\mu\varepsilon$ via finite element method. Different color in each grid indicats the value of stress and displacement in the grid. White dash line denotes the origin interface between the two spliced fibers. Black dash line denotes the position of fiber cores.

with the increased tensile strain, as shown in Fig. 3(b). So the fiber in-line MZI can be used to develop a promising intensity-modulated strain sensor with a high sensitivity of -0.023 dBm/$\mu\varepsilon$. Meanwhile, according to Eq.2, the dip wavelength of interference fringes maintain steadily because it does not depend on the splitting ratio of light.

Simulation results show that, providing the applied tensile strain is increased over a threshold of 500 $\mu\varepsilon$, such a strain hardly induces further physical deformation and refractive index change. In other words, a large tensile strain mainly results in an extension of the MZI cavity length, rather than of a change of the splitting ratio of light. As a result, the dip intensity is insensitive to the applied strain of more than 500 $\mu\varepsilon$, whereas the dip wavelength linearly shifted toward a shorter wavelength, as shown in Fig. 3(b). The reason of this phenomenon is that, according to Eq. 2, the increase of the MZI cavity length, $\Delta n_{eff,\varepsilon} \cdot \delta L$, has a weaker impact on the dip wavelength than the decrease of effective refractive index difference, $-\delta n_{eff,\varepsilon} \cdot L$ [7], [9] so that the dip wavelength will 'blue' shift while the tensile strain increases over 500 $\mu\varepsilon$.

IV. Conclusion

In conclusion, a novel fiber in-line MZI with a misalignment-spliced joint was demonstrated to develop a promising intensity-modulated strain sensor. Such a strain sensor exhibited an ultrahigh sensitivity of -0.023 dBm/$\mu\varepsilon$ within a strain range of less than 500 $\mu\varepsilon$, which is about

one order of magnitude higher than the reported values. And a strain resolution of 0.43 $\mu\varepsilon$ could be achieved. The fiber in-line MZI can also be used to measure a large tensile strain of more than 500 $\mu\varepsilon$ by means of wavelength modulation with a high sensitivity of -1.78 pm/$\mu\varepsilon$. Furthermore, our MZI-based sensor presents the merits of compact size (only 10 mm), high sensitivities, good repeatability, and good mechanical reliability. Hence, it is expected to have a good practical application in strain measurement fields.

REFERENCES

[1] J. Dakin and B. Culshaw, *Optical Fiber Sensors: Principles and Components*. Norwood, MA, USA: Artech House, 1988.

[2] K. T. V. Grattan and B. T. Meggitt, *Optical Fiber Sensor Technology*. London, U.K.: Chapman & Hall, 1995.

[3] B. Lee, "Review of the present status of optical fiber sensors," *Opt. Fiber Technol.*, vol. 9, no. 2, pp. 57–79, 2003.

[4] E. B. Li, X. L. Wang, and C. Zhang, "Fiber-optic temperature sensor based on interference of selective higher-order modes," *Appl. Phys. Lett.*, vol. 89, pp. 091119-1–091119-3 Aug. 2006.

[5] A. B. Socorro, I. Del Villar, J. M. Corres, F. J. Arregui, and I. R. Matias, "Mode transition in complex refractive index coated single-mode-multimode-single-mode structure," *Opt. Express*, vol. 21, pp. 12668–12682, May 2013.

[6] L. V. Nguyen, D. Hwang, S. Moon, D. S. Moon, and Y. Chung, "High temperature fiber sensor with high sensitivity based on core diameter mismatch," *Opt. Express*, vol. 16, pp. 11369–11375, Jul. 2008.

[7] P. Lu and Q. Chen, "Asymmetrical fiber Mach–Zehnder interferometer for simultaneous measurement of axial strain and temperature," *IEEE Photon. J.*, vol. 2, no. 6, pp. 942–953, Dec. 2010.

[8] G. L. Yin, S. Q. Lou, and H. Zou, "Refractive index sensor with asymmetrical fiber Mach–Zehnder interferometer based on concatenating single-mode abrupt taper and core-offset section," *Opt. Laser Technol.*, vol. 45, pp. 294–300, Feb. 2013.

[9] P. Lu, L. Men, K. Sooley, and Q. Chen, "Tapered fiber Mach–Zehnder interferometer for simultaneous measurement of refractive index and temperature," *Appl. Phys. Lett.*, vol. 94, pp. 131110-1–131110-3, 2009.

[10] Z. Wu, *et al.*, "In-line Mach–Zehnder interferometer composed of microtaper and long-period grating in all-solid photonic bandgap fiber," *Appl. Phys. Lett.*, vol. 101, pp. 141106-1–141106-4, Oct. 2012.

[11] Y. P. Wang, Y. J. Rao, Z. L. Ran, T. Zhu, and X. K. Zeng, "Bend-insensitive long-period fiber grating sensors," *Opt. Lasers Eng.*, vol. 41, pp. 233–239, Jan. 2004.

[12] Y. P. Wang, "Review of long period fiber gratings written by CO_2 laser," *J. Appl. Phys.*, vol. 108, pp. 081101-1–081101-18, Oct. 2010.

[13] Y. J. Rao, Y. P. Wang, Z. L. Ran, T. Zhu, and B. Yu, "Characteristics of novel long-period fibre gratings written by focused high-frequency CO_2 laser pulses," *Proc. SPIE*, vol. 4581, pp. 327–333, Nov. 2001.

[14] L. Zhao, L. Jiang, S. Wang, H. Xiao, Y. Lu, and H.-L. Tsai, "A high-quality Mach–Zehnder interferometer fiber sensor by femtosecond laser one-step processing," *Sensors*, vol. 11, pp. 54–61, Jan. 2011.

[15] C. R. Liao, Y. Wang, D. N. Wang, and M. W. Yang, "Fiber in-line Mach–Zehnder interferometer embedded in FBG for simultaneous refractive index and temperature measurement," *IEEE Photon. Technol. Lett.*, vol. 22, no. 22, pp. 1686–1688, Nov. 15, 2010.

[16] X. Xing, Y. Wang, and B. Li, "Nanofibers drawing and nanodevices assembly in poly (trimethylene terephthalate)," *Opt. Express*, vol. 16, no. 14, pp. 10815–10822, 2008.

[17] Y. H. Li and L. M. Tong, "Mach–Zehnder interferometers assembled with optical microfibers or nanofibers," *Opt. Lett.*, vol. 33, no. 4, pp. 303–305, 2008.

[18] R. Jha, J. Villatoro, G. Badenes, and V. Pruneri, "Refractometry based on a photonic crystal fiber interferometer," *Opt. Lett.*, vol. 34, pp. 617–619, Mar. 2009.

[19] W. Zhou, W. C. Wong, C. C. Chan, L.-Y. Shao, and X. Dong, "Highly sensitive fiber loop ringdown strain sensor using photonic crystal fiber interferometer," *Appl. Opt.*, vol. 50, pp. 3087–3092, Jul. 2011.

[20] J. Zheng, *et al.*, "Temperature and index insensitive strain sensor based on a photonic crystal fiber in line Mach–Zehnder interferometer," *Opt. Commun.*, vol. 297, pp. 7–11, Jun. 2013.

[21] C. Shen, *et al.*, "Temperature-insensitive strain sensor using a fiber loop mirror based on low-birefringence polarization-maintaining fibers," *Opt. Commun.*, vol. 287, pp. 31–34, Jan. 2013.

[22] L. V. Nguyen and Y. Chung, "All-optical signal gating using ytterbium-doped fiber and a pair of thermally expanded core fibers," *Appl. Phys. Lett.*, vol. 95, pp. 161111-1–161111-3, Oct. 2009.

[23] B. Dong, D.-P. Zhou, and L. Wei, "Temperature insensitive all-fiber compact polarization-maintaining photonic crystal fiber based interferometer and its applications in fiber sensors," *J. Lightw. Technol.*, vol. 28, no. 7, pp. 1011–1015, Apr. 1, 2010.

[24] Y. P. Wang, J. P. Chen, X. W. Li, J. X. Hong, and X. H. Zhang, "Measuring electro-optic coefficients of poled polymers using fiber-optic Mach–Zehnder interferometer," *Appl. Phys. Lett.*, vol. 85, no. 21, pp. 5102–5103, 2004.

[25] Y. J. Rao, X. K. Zeng, and Y. Zhu, "Temperature-strain discrimination sensor using a WDM chirped in-fibre Bragg grating and an extrinsic Fabry-Pérot," *Chin. Phys. Lett.*, vol. 18, pp. 643–645, May 2001.

[26] C. R. Liao, D. N. Wang, M. Wang, and M. Yang, "Fiber in-line Michelson interferometer tip sensor fabricated by femtosecond laser," *IEEE Photon. Technol. Lett.*, vol. 24, no. 22, pp. 2060–2063, Nov. 15, 2012.

[27] W. Qian, C.-L. Zhao, X. Dong, and W. Jin, "Intensity measurement based temperature-independent strain sensor using a highly birefringent photonic crystal fiber loop mirror," *Opt. Commun.*, vol. 283, no. 24, pp. 5250–5254, 2010.

[28] M. S. Yoon, S. Park, and Y. G. Han, "Simultaneous measurement of strain and temperature by using a micro-tapered fiber grating," *J. Lightw. Technol.*, vol. 30, no. 8, pp. 1156–1160, Apr. 15, 2012.